RESEARCH ARTICLE OPEN ACCESS

Design and Implementation of Power Converters for Hybrid Wind-Solar Energy Conversion System with an Implementation of MPPT

G. Sridhar Babu*, Y. Kanakaraju**
*(Department of Electrical and Electronics, Asst.Professor M.Tech (P.E), S.M.E.C affiliated to J.N T.U Hyderabad)
** (Student of S.M.E.C, M.tech (P.E))

Abstract
This paper presents the design and implementation of power converters for wind conversion systems. The power converter can not only transfer the power from a wind generator, but also improve the stability and safety of the system. The proposed system consists of a Permanent magnet synchronous generator (PMSG); a DC/DC boosts converter, a bi-directional DC/DC converter and a full-bridge DC/AC inverter. The wind generator is the main power source of the system, and the battery is used for energy storage and power compensation to recover the natural irregularity of the wind power. In this paper presents a new system configuration of the front-end rectifier stage for a hybrid wind or photo voltaic energy system. The configuration allows the two sources to supply the load separately or simultaneously, depending on the availability of energy sources. The inherent nature of this cuk-scpic fused converter, additional input filters are not necessary to filter out high frequency harmonic content is determinant for the generator life span, heating issue and efficiency. The fused multi-input rectifier stage also allows maximum power from the wind and sun. When it is available an adaptive MPPT algorithm will be used for photo voltaic (PV) system. Operational analysis of the proposed system, will discoursed in this paper simulation results are given to highlight the merit of the proposed circuit

Index terms —Wind generator, PV and Fuel Cells, Bi-directional DC/DC converter, full-bridge DC/AC inverter, MPPT.

I. INTRODUCTION

With increasing concern of global warming and the depletion of fossil fuel reserves, many are looking at sustainable energy solutions to preserve the earth for the future generations. Other than hydro power, wind and photovoltaic, fuel cells energy holds the most potential to meet our energy demands. Alone, wind energy is capable of supplying large amounts of power but its presence is highly unpredictable as it can be here one moment and gone in another. Similarly, solar energy is present throughout the day but the solar irradiation levels vary due to sun intensity and unpredictable shadows cast by clouds, birds, trees, etc. The common inherent drawback of wind and photovoltaic systems are their intermittent natures that make them unreliable. However, by combining these two intermittent sources and by incorporating maximum power point tracking (MPPT) algorithms, the system's power transfer efficiency and reliability can be improved significantly.

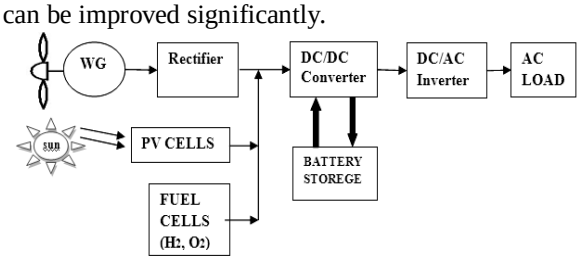

Fig. 1 the diagrams of Hybrid wind-Solar systems

When a source is unavailable or insufficient in meeting the load demands, the other energy source can compensate for the difference. Several hybrid wind/PV power systems with MPPT control have been proposed and discussed in works. Most of the systems in literature use a separate DC/DC boost converter connected in parallel in the rectifier stage as to perform the MPPT control for each the renewable energy power sources. A simpler multi input structure has been suggested by that combine the sources from the DC-end while still achieving MPPT for each renewable source. The systems in literature require passive input filters to remove the high frequency current harmonics injected into wind turbine generators. The harmonic content in the generator current decreases its lifespan and increases the power loss due to heating.

The proposed design is a fusion of the Cuk and SEPIC converters. The features of the proposed topology are: 1) the inherent nature of these two converters eliminates the need for separate input filters for PFC; 2) it can support step up/down operations for each renewable source (can support wide ranges of PV and Wind input); 3) MPPT can be realized for each source; 4) individual and simultaneous operation is supported. The circuit operating principles will be discussed in this paper. Simulation results are provided to verify with the feasibility of the proposed system.

The characteristics of the wind generator are described in section II. The system construction and the flexible control strategy of the power converters are depicted in section III. The performance of power converters and the flexibility of control strategy will be in section IV. The MPPT control of proposed circuit in section V. the simulation results in section VI. Conclusions are made in Section VII.

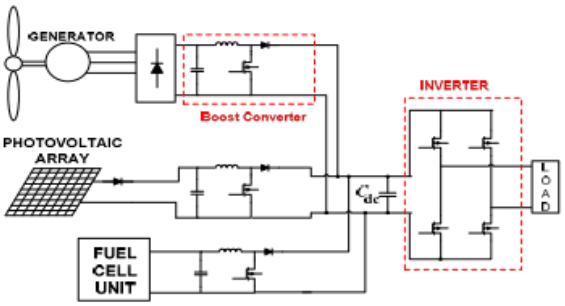

Figure 2: Hybrid system with multi-connected boost converter

II. CHARACTERISTICS OF WIND GENERATOR

The wind turbine depends on the flow of air in a rotor consisting of two or three blades mechanically coupled to an electrical generator. It is a process of power translation from wind energy to electricity. The difference between the upstream and downstream wind powers is actual power extracted by the rotor blades,. It is given by the following equation in units of watts.

$$\mathbf{P_m = \frac{1}{2}\ m^*\left\{V^2 - V_0^2\right\}} \quad (1)$$

Where P_M is mechanical power extracted by the rotor, that is the turbine power, and V is upstream wind velocity at the entrance of the rotor blades and V_O is downstream wind velocity at the exit of the rotor blades. Multiplying the air density by the average velocity, therefore, gives the mass flow rate (m^*) of air through the rotating blades, which is as follows:

$$\boldsymbol{m^* = \rho A\frac{V + V_0}{2}} \quad (2)$$

Where is air density (typically 1.25 kg/m3), and A is a area swept by the rotor blades (m2). Applying (2) into (1), (1) can be written as

$$\boldsymbol{P_m = \frac{1}{2}[\rho A\frac{V+V_0}{2}]\{V^2 - V_0^2\}} \quad (3)$$

Rewriting (3) gives

$$\boldsymbol{P_m = \frac{1}{2}\rho A V^3\frac{\left(1+\frac{V_0}{V}\right)\left[1-\left(\frac{V_0}{V}\right)^2\right]}{2}} \quad (4)$$

Assuming R is the blade radius (m), (4) can be expressed as

$$\boldsymbol{P_m = \frac{1}{2}\pi R^2\rho V^3\frac{\left(1+\frac{V_0}{V}\right)\left[1-\left(\frac{V_0}{V}\right)^2\right]}{2}} \quad (5)$$

It is a proportional relationship between the power extracted by the wind turbine and the rotor efficiency. (5) Can be rewritten as

$$\mathbf{p_m = \frac{1}{2}\pi R^2\rho V^3 C_P} \quad (6)$$

Where *CP* is the wind turbine rotor efficiency which is given by the following expression:

$$\boldsymbol{C_P = \frac{\left(1+\frac{V_0}{V}\right)\left[1-\left(\frac{V_0}{V}\right)^2\right]}{2}} \quad (7)$$

The power extracted by the wind turbine increases with the raise of *C*. However, *CP* is limited by the aeromechanics and it is maximum value is 16/27 in theory. In other words, the maximum power coefficient of the power extracted by rotor blades is about 59%. *C* is also affected by the variation of the generator tip-speed-ratio (TSR) as follows:

$$\boldsymbol{\lambda = \frac{\omega R}{V}} \quad (8)$$

Where is the WG rotor speed of rotation (rad/s), R is the radius of the area swept by wind turbine blades. Theoretically, the maximum power point of a generator corresponds to a value of TSR at different wind speeds. Therefore, when the wind speed is fixed, a non-linear relationship between the generator output power and the rotor speed are shown in Fig .3

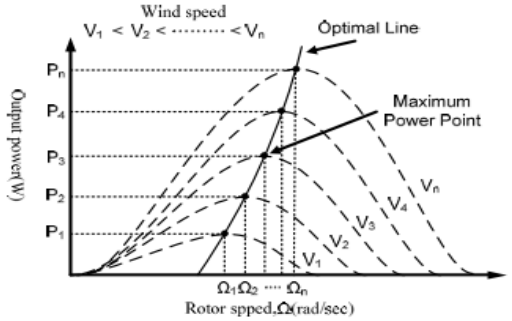

Fig. 3: the WG output power curves at various wind speeds

A variable-speed operation of the wind generators to enables the system to effectively reduce the mechanical stress on the generator blades and gears. In addition, the design of the system structure and control strategy has a great influence on the system performance and the power output of generator [6].

III.PROPOSED MULTI-INPUT CONVERTERS

A system diagram of the proposed rectifier stage of a hybrid energy system is shown in Figure 2, where one of the inputs is connected to the output of the PV array and the other input connected to the output of a generator. The fusion of the two converters is achieved by reconfiguring the two existing diodes from each converter and the shared utilization of the Cuk output inductor by the SEPIC converter. This configuration allows each converter to operate normally individually in the event that one source is unavailable. Figure 3 illustrates the case when only the wind source is available. In this case, d_1 turns off and d_2 turns on; the proposed circuit becomes a SEPIC converter and the input to output voltage relationship is given by (1). On the other hand, if only the PV source is available, then d_2 turns off and d_1 will always be on and the circuit becomes a Cuk converter as shown in Figure 4. The input to output voltage relationship is given by (2). In both cases, both converters have step-up/down capability, which provide more design flexibility in the system if duty ratio control is utilized to perform MPPT control.

$$\frac{V_{dc}}{V_w} = \frac{d_2}{1-d_1} \quad (1)$$

$$\frac{V_{dc}}{V_w} = \frac{d_1}{1-d_1} \quad (2)$$

Figure 7 illustrates the various switching states of the proposed converter. If the turn on duration of M_1 is longer than M_2, then the switching states will be state I, II, IV. Similarly, the switching states will be state I, III, IV if the switch conduction periods are vice versa. To provide a better explanation, the inductor current waveforms of each switching state are given as follows assuming that $d_2 > d_1$; hence only states I, III, IV are discussed in this example. In the following, $I_{i,\,PV}$ is the average input current from the PV source; I is the RMS input current after the rectifier (wind case); and $I_{i,w}$ is the average system output current. The key waveforms that illustrate the switching states in this example are shown in Figure 8. The mathematical expression that relates the total output voltage and the two input sources will be illustrated in the next section.

State I (M_1 *on*, M2 *on*):

$$i_{L1} = I_{i,PV} + \frac{V_{PV}}{L_1} t \qquad 0<t<d_1T_s$$

$$i_{L2} = I_{dc} + \left(\frac{V_{c1}+V_{C2}}{L_2}\right) t \qquad 0<t<d_1T_s$$

$$i_{L3} = I_{i,w} + \frac{V_w}{L_3} t \qquad 0<t<d_1T_s$$

State III (M_1*off*, M2 *on*):

$$i_{L1} = I_{i,pv} + \left(\frac{V_{PV}-V_{C1}}{L_1}\right) t \qquad d_1T_s<t<d_2T_{/s}$$

$$i_{L2} = I_{dc} + \frac{V_{c2}}{L_2} t \qquad d_1T_s<t<d_2T_{/s}$$

$$i_{L3} = I_{i,w} + \frac{V_w}{L_3} t \qquad d_1T_s<t<d_2T_{/s}$$

State IV (M_1 *off*, M_2 *ff):*

$$i_{L1} = I_{i,pv} + \left(\frac{V_{PV}-V_{C1}}{L_1}\right) t \qquad d_2T_s<t< T_s$$

$$i_{L2} = I_{dc} - \frac{V_{dc}}{L_2} t \qquad d_2T_s<t< T_s$$

$$i_{L3} = I_{i,w} + \left(\frac{V_w-V_{c2}-V_{dc}}{L_3}\right) t \qquad d_2T_s<t< T_s$$

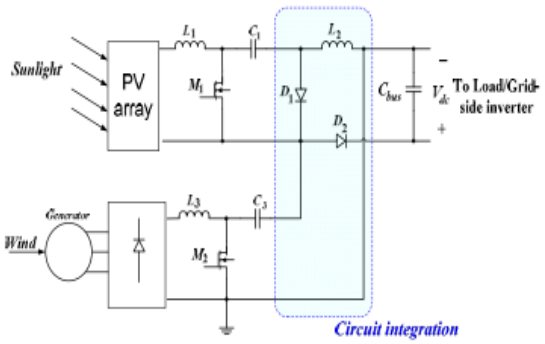

Figure 4: Proposed rectifier stage for a Hybrid wind/PV system

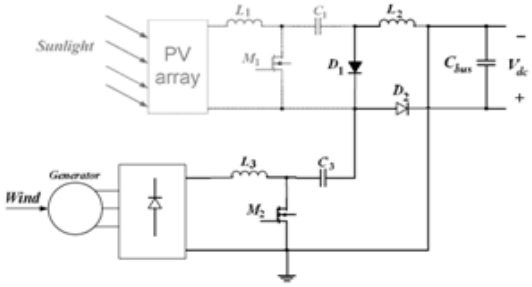

Figure 5: Only wind source is operational (SEPIC)

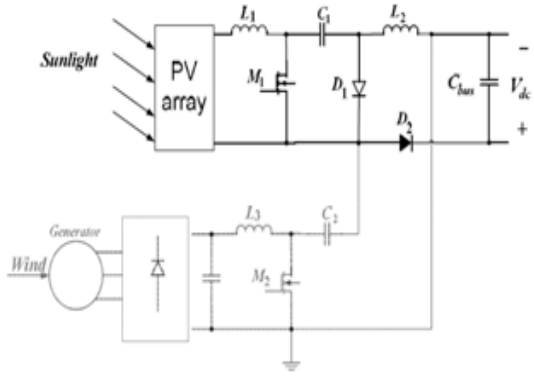

Figure 6: Only PV source is operation (Cuk)

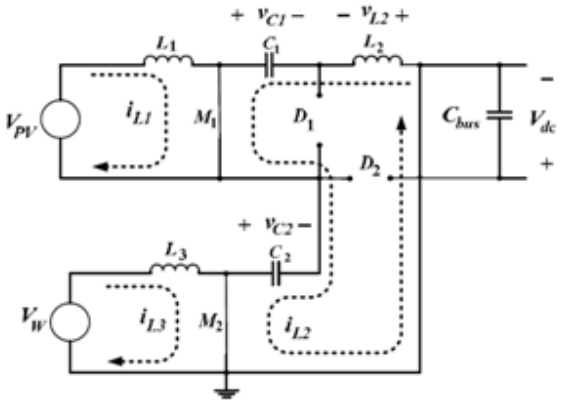

(1)

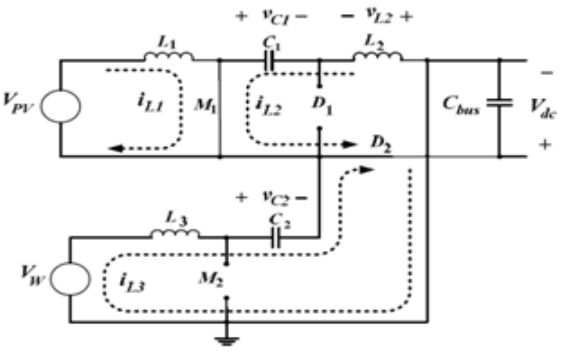

(2)

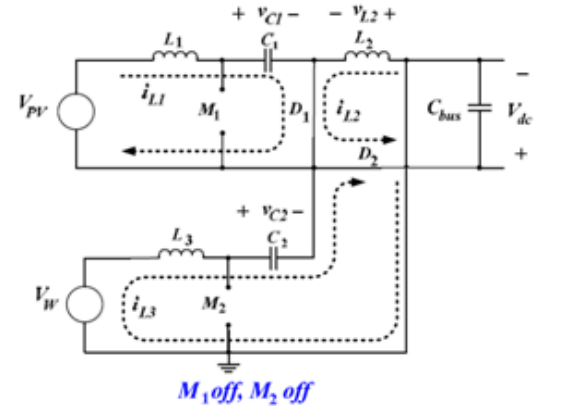

(3)

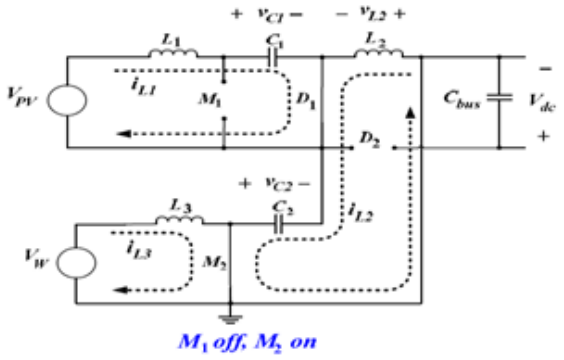

(4)

From (1–4)

Figure: 7: switching states within a switching cycle

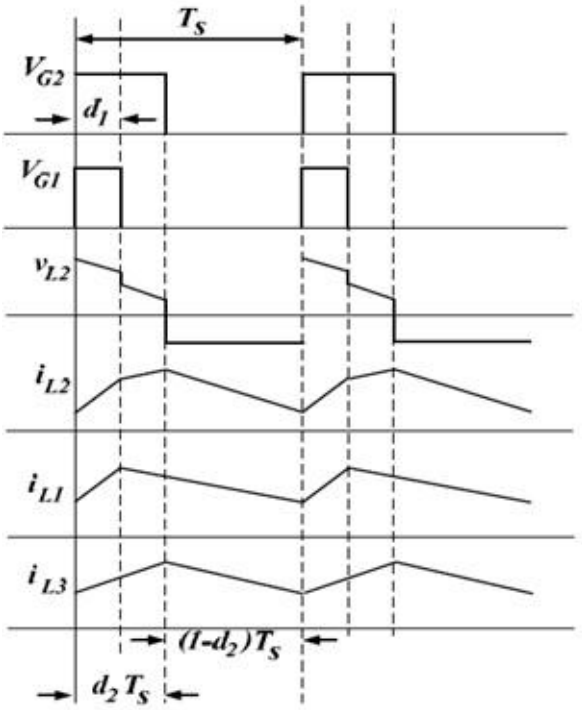

Figure 8: Proposed circuit inductor waveforms

III. ANALYSIS OF PROPOSED CIRCUIT

To find an expression for the output dc bus voltage, V, the volt-balance of the output inductor, L, is examined according to Figure8 with $d_2 > d_1$. Since the net change in the voltage of L_2 is zero, applying volt-balance to L results in (3). The expression that relates the average output dc voltage(V_{dc}) to the capacitor voltages (V_{c1} and V_{c2}) is then obtained as shown in (4), where *vc*1 and *v* can then be obtained by applying volt-balance to L_1 and L_{c2} [9]. The final expression that relates the average output voltage and the two input sources (V_W and V_{PV}) is then given by (5). It is observed that V is simply the sum of the two output voltages of the Cuk and SEPIC converter. This further implies that V_{dc} can be controlled by d_1 and d_2 individually or simultaneously.

$$(v_{c1}+v_{c2})d_1T_s+(v_{c2})(d_2-d_1)T_s+(1-d_2)(-V_{dc})T_s=0$$

$$V_{dc} = \left(\frac{d_1}{1-d_2}\right)v_{c1} + \left(\frac{d_2}{1-d_2}\right)v_{c2} \quad (4)$$

$$V_{dc} = \left(\frac{d_1}{1-d_2}\right)V_{PV} + \left(\frac{d_2}{1-d_2}\right)V_w \quad (5)$$

The switches voltage and current characteristics are also provided in this section. The voltage stress is given by (6) and (7) respectively. As for the current stress, it is observed from Figure 6 that the peak current always occurs at the end of the on-time of the MOSFET. Both the Cuk and SEPIC MOSFET current consists of both the input current and the capacitors (C_1or C_2) current. The peak current stress of $M1$ and M are given by (8) and (10)

respectively.Leq1 and L, given by (9) and (11), represent the equivalent inductance of Cuk and SEPIC converter respectively.

The PV output current, which is also equal to the average input current of the Cuk converter, is given in (12). It can be observed that the average inductor current is a function of its respective duty cycle (*d*). Therefore by adjusting the respective duty cycles for each energy source, maximum power point tracking can be achieved. 1

$$\boldsymbol{v_{ds1} = V_{pv}\left(1 + \frac{d_1}{1-d_1}\right)} \quad (6)$$

$$\boldsymbol{v_{ds1} = V_{pv}\left(1 + \frac{d_2}{1-d_2}\right)} \quad (7)$$

$$\boldsymbol{i_{ds1,pk} = I_{i,PV} + I_{dc,avg} + \frac{V_{pv} d_1 T_s}{2L_{eq2}}} \quad (8)$$

$$\boldsymbol{L_{eq2} = \frac{L_1 L_2}{L_1 + L_2}} \quad (9)$$

$$\boldsymbol{i_{ds2,pk} = I_{i,w} + I_{dc,avg} + \frac{V_w d_2 T_s}{2L_{eq1}}} \quad (10)$$

$$\boldsymbol{L_{eq2} = \frac{L_3 L_2}{L_3 + L_2}} \quad (11)$$

$$\boldsymbol{I_{i,PV} = \frac{p_0}{V_{dc}}\left(\frac{d_1}{1-d_1}\right)} \quad (12)$$

V.MPPT CONTROL OF PROPOSED CIRCUIT

A common inherent drawback of wind and PV systems is the intermittent nature of their energy sources. Wind energy is capable of supplying large amounts of power but its presence is highly unpredictable as it can be here one moment and gone in another. Solar energy is present throughout the day, but the solar irradiation levels vary due to sun intensity and unpredictable shadows cast by clouds, birds, trees, etc. These drawbacks tend to make these renewable systems inefficient. However, by incorporating maximum power point tracking (MPPT) algorithms, the systems' power transfer efficiency can be improved significantly. To describe a wind turbines power characteristic, equation (13) describes the mechanical power that is generated by the wind [6].

$$\boldsymbol{P_m = 0.5 \rho A C_p(\lambda, \beta) V_w^3} \quad (13)$$

Where

ρ = air density
A = area swept by rotor
Cp (λ, β) = power coefficient
V_w^3 = Wind Speed
λ = Tip Speed ratio,
β = Pitch Angle

The power coefficient (C_P) is a nonlinear function that represents the efficiency of the wind turbine to convert wind energy into mechanical energy. It is dependent on two variables, the tip speed ratio (TSR) and the pitch angle. The TSR, **λ**, refers to a ratio of the turbine angular speed over the wind speed. The mathematical representation of the TSR is given by (14). The pitch angle, ß, refers to the angle in which the turbine blades are aligned with respect to its longitudinal axis.

$$\boldsymbol{\lambda = \frac{R\omega_b}{V_w}} \quad (14)$$

Where

R = turbine radius,
ω_b = angular rotational speed

Figure 9 and 10 are illustrations of a power coefficient curve and power curve for a typical fixed pitch (ß =0) horizontal axis wind turbine. It can be seen from figure 7 and 8 that the power curves for each wind speed has a shape similar to that of the power coefficient curve. Because the TSR is a ratio between the turbine rotational speed and the wind speed, it follows that each wind speed would have a different corresponding optimal rotational speed that gives the optimal TSR. For each turbine there is an optimal TSR value that corresponds to a maximum value of the power coefficient (C*b*) and therefore the maximum power. Therefore by controlling rotational speed, (by means of adjusting the electrical loading of the turbine generator) maximum power can be obtained for different wind speeds.

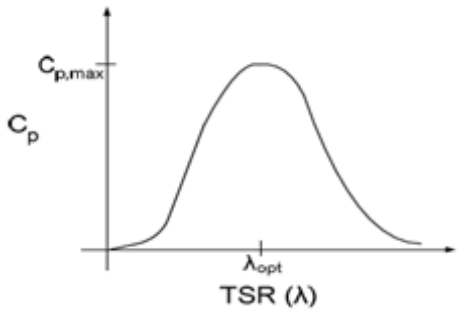

Figure 9: Power Coefficient Curve for a typical wind turbine

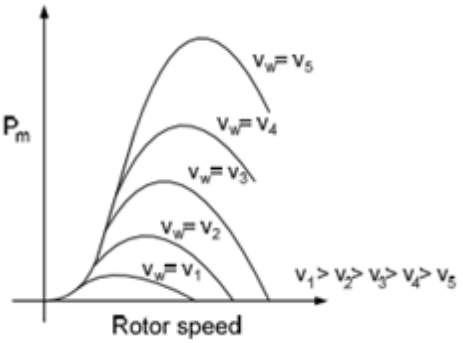

Figure 10: Power Curves for a typical wind turbine

A solar cell is comprised of a P-N junction semiconductor that produces currents via the photovoltaic effect. PV arrays are constructed by placing numerous solar cells connected in series and in parallel. A PV cell is a diode of a large-area forward bias with a photo voltage and the equivalent circuit is shown by Figure 11. The current-voltage characteristic of a solar cell is derived in [12] and [13] as follows:

$$\boldsymbol{I = I_{ph} - I_D} \quad (15)$$

$$\boldsymbol{I = I_{ph} - I_0[exp\left(\frac{q(V+R_sI)}{ATk_B}\right) - 1] - \frac{V+R_sI}{R_{sh}}} \quad (16)$$

Where

Iph = photocurrent,
I_D= diode current,
I_O= saturation current,
A = ideality factor,
q = electronic charge 1.6x10-9,
Kg = Boltzmann's gas constant ($1.38x10^{-23}$)
T = cell temperature,
R_s = series resistance,
R_{sh} = shunt resistance,
I = cell current, V = cell voltage

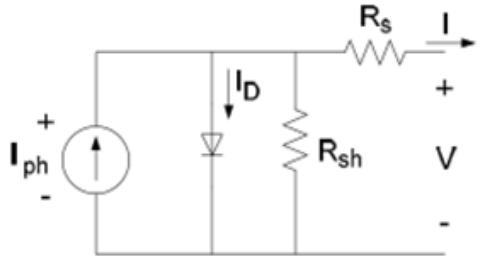

Figure 11: PV cell equivalent circuit

Typically, the shunt resistance (R_{sh}) is very large and the series resistance (R_s) is very small. Therefore, it is common to neglect these resistances in order to simplify the solar cell model. The resultant ideal voltage-current characteristic of a photovoltaic cell is given by (17) and illustrated by Figure 12.

$$\boldsymbol{I = I_{ph} - I_0[exp\left(\frac{qv}{kT}\right) - 1]} \quad (17)$$

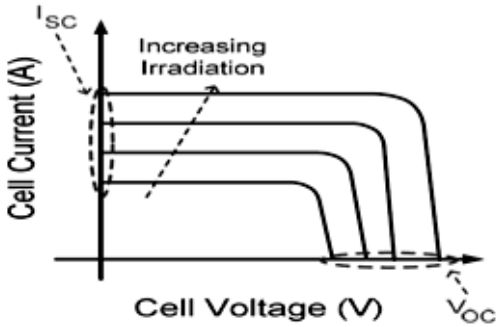

Figure 12: PV cell voltage-current characteristic

The typical output power characteristics of a PV array under various degrees of irradiation is illustrated by Figure 13. It can be observed in Figure 11 that there is a particular optimal voltage for each irradiation level that corresponds to maximum output power. Therefore by adjusting the output current (or voltage) of the PV array, maximum power from the array can be drawn.

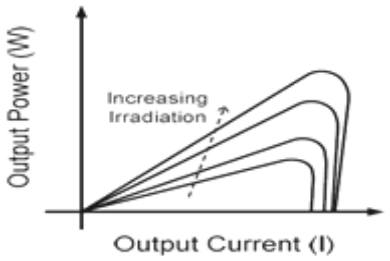

Figure 13: PV cell power characteristics

Due to the similarities of the shape of the wind and PV array power curves, a similar maximum power point tracking Scheme known as the hill climb search (HCS) strategy is often applied to these energy sources to extract maximum Power. The HCS strategy perturbs the operating point of the system and observes the output. If the direction of the Perturbation (e.g an increase or decrease in the output voltage of a PV array) results in a positive change in the output power, then the control algorithm will continue in the direction of the previous perturbation. Conversely, if a negative change in the output power is observed, then the control algorithm will reverse the direction of the pervious Perturbation step. In the case that the change in power is close to zero (within a specified range) then the algorithm will invoke no changes to the system operating point since it corresponds to the maximum power point (the peak of the power curves). The MPPT scheme employed in this paper is a version of the HCS strategy and flow chart that illustrates the implemented MPPT.

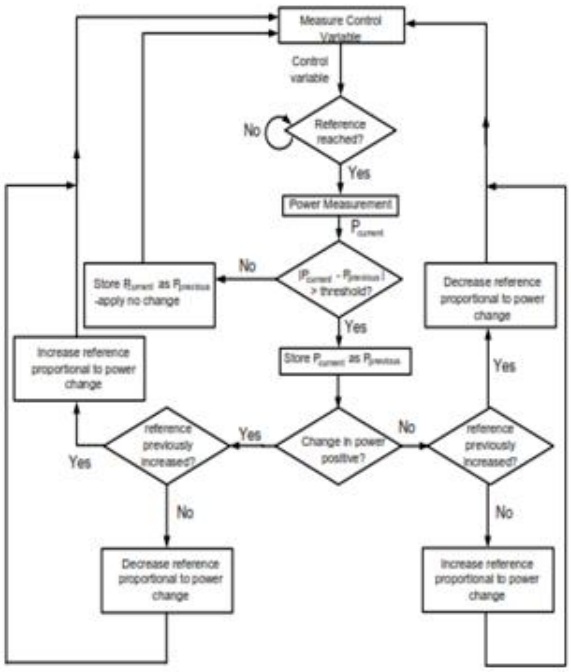

Figure 14: General MPPT Flow Chart for wind and PV

VI.SIMULATION CIRCUTS & RESULTS

In this section, a simulation result is given to verify that the proposed multi-input converters can support individual as well as simultaneous operation. Figure 22 illustrates the system under the condition where the wind source has failed and only the PV source (Cuk converter mode) is supplying power to the load. Figure 17 illustrates the system where only the wind turbine generates power to the load (SEPIC converter mode). Finally, Figure 24 illustrates the simultaneous Operation of hybrid wind-solar energy system output power shown.

CIRCUITS:

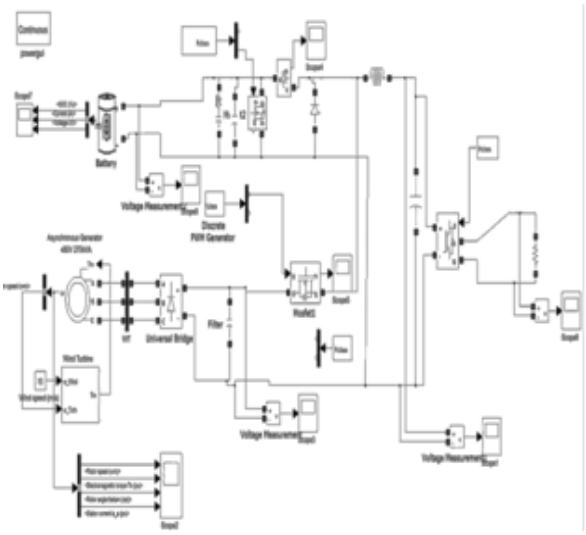

Figure 15: Simulation Diagram of Wind Energy Conversion system

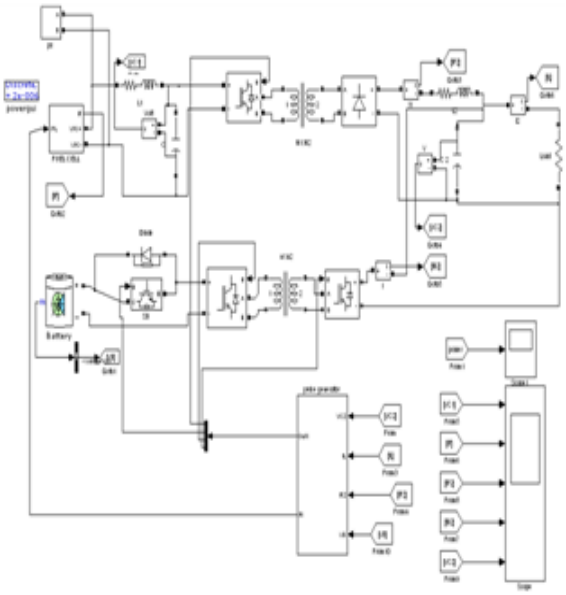

Figure 16: Simulation Diagram of Hybrid PV, Fuel Cell system

RESULTS:

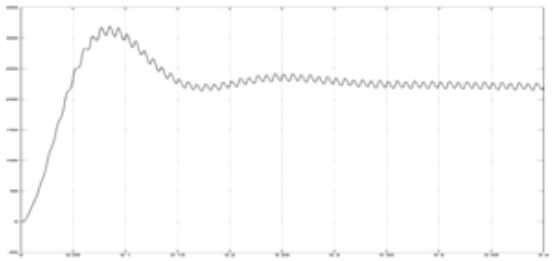

Figure 17: wind energy output current at load

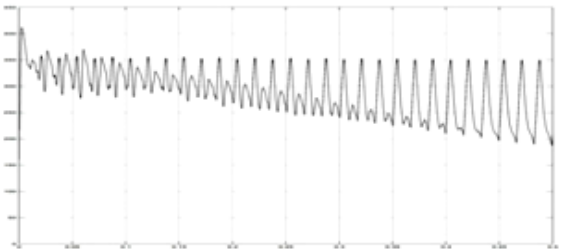

Figure18: Wind Generator Output Voltage at load

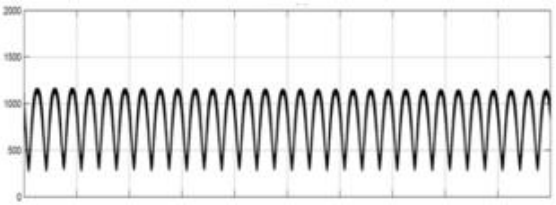

(i)

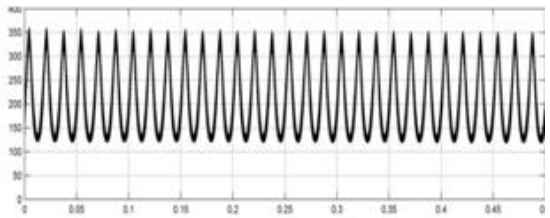

(ii)

Figure 19 :(i), (ii) Simulation files running condition: The generator current & Voltage

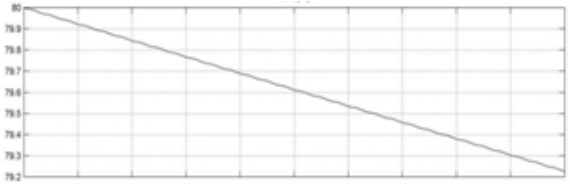

Figure 20: wind System output current

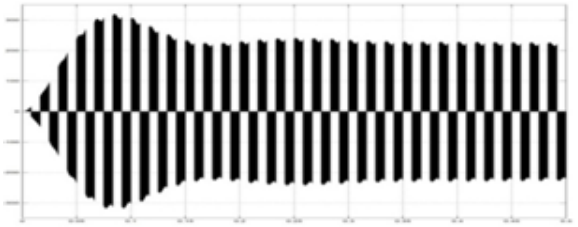

Figure 21: Wind MPPT – Generator speed and Reference speed signal (SEPIC operation)

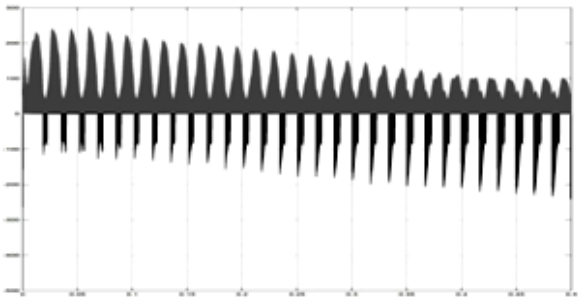

Figure 22: Individual operation with only wind source (SEPIC) Top: Output power, Bottom: Switch currents (M1 and M2)

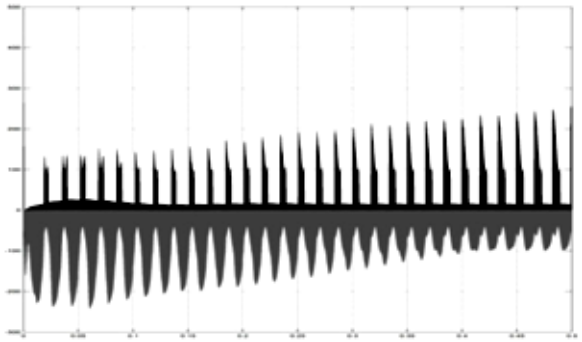

Figure 23: Individual operation with only PV source (Cuk) Top: Output power, Bottom: Switch currents (M1 and M2)

The injected three phase generator current (EPIC, Cuk)

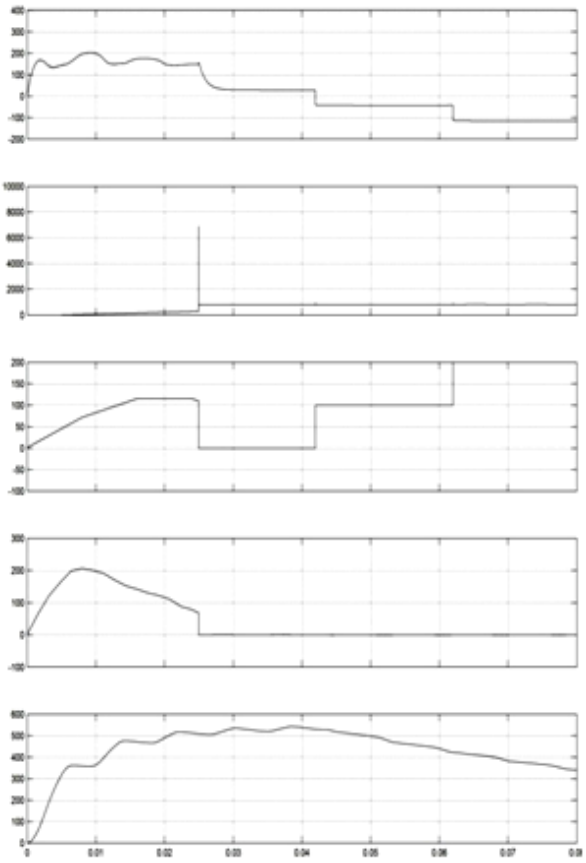

Figure 24: Output load power of Hybrid system

VII. CONCLUSION

In this a new multi-input Cuk-SEPIC rectifier stage for hybrid wind/solar energy systems has been presented. The features of this circuit are: 1) additional input filters are not necessary to filter out high frequency harmonics; 2) both renewable sources can be stepped up/down (supports wide ranges of PV and wind input); 3) MPPT can be realized for each source; 4) individual and simultaneous operation is supported. Simulation results have been presented to verify the features of the proposed topology.

By implementing this technique we can increase the power transfer efficiency. We can extract maximum power without any interruption. There is no need to depend upon non renewable energy sources and this is eco friendly

REFERENCES

[1] An Integrated Hybrid Power Supply for Distributed Generation Applications Fed by Nonconventional Energy Sources. Sachin Jain and Vivek Agarwal, *Senior Member IEEE* vol. 23, No. 2, JUNE 2008

[2] Control Strategy for a Variable-Speed Wind Turbine Using DC Bus Measurements, SISY 2010, IEEE 8th International Symposium on Intelligent Systems and Informatics • September 10-11, 2010 by C. Koch-Ciobotaru, R. Boraci, I. Filip, C. Vasar, G. Prostean

[3] Compensation Loop Design of A Photovoltaic System Based on Constant Voltage MPPT 978-1-4244-2487-0/09/$25.00 ©2009 IEEE by Hangzhou, China

[4] An Efficient AC–DC Step-Up Converter for Low-Voltage Energy Harvesting by Suman Dwari, *Student Member, IEEE*, and Leila Parsa, *Member*, IEEE Transactions on Power Electronics, Vol. 25, No. 8, Aug 2010.

[5] Dynamic Maximum Power Point Tracking of Photovoltaic Arrays Using Ripple Correlation Control Trishan Esram, Jonathan W. Kimball , Philip T. Krein IEEE Transaction on Power Electronics, Vol. 21, No. 5, September 2006.

[6] R. Kyoungsoo and S. Rahman, "Two loop controller for maximizing performanceof a grid-connected, photovoltaic fuel cell hybrid power plant,"*IEEE Trans. Energy Convers.*, vol. 13, no. 3, pp. 276–281, Sep. 1998.

[7] F. Valenciaga and P. F. Puleston, "Supervisor control for a stand-alone hybrid generation system using wind and photovoltaic energy," *IEEE Trans. Energy Convers.*, vol. 20, no. 2, pp. 398–405, Jun. 2005.62

[8] N. Kato, K. Kurozumi, N. Susuld, and S. Muroyama, "Hybrid power supply system composed of photovoltaic and fuel-cell systems," in *Telecommun. Energy Conf.*, Jpn, Oct., 2001, pp. 631–635.

[9] T. Senjyu, T. Nakaji, K. Uezato, and T. Funabashi, "A hybrid power system using alternative energy facilities in isolated island," *IEEE Trans. Energy Convers.*, vol. 20, no. 2, pp. 406–414, Jun. 2005.

[10] Y. M. Chen, C. S. Cheng, and H. C.Wu, "Grid-connected hybrid PV/wind power generation system with improved dc bus voltage regulation strategy," in *Proc. IEEE APEC*, 2006, pp. 1089–1094.

[11] W. Gao, "Performance comparison of a fuel cell-battery hybrid power train and a fuel cell-ultra capacitor hybrid power train," *IEEE Trans. Veh. Technol.*, vol. 54, no. 3, pp. 846–855, May 2005.

[12] H. Tao, A. Kotsopoulos, J. L. Duarte, and M. A.M. Hendrix, "Multi-input bidirectional dc–dc converter combining dc-link and magnetic coupling for fuel cell systems," in *Proc. IEEE Conf. Ind. Appl.*, 2003, vol. 3, pp. 1136–1142.

[13] Power Management of a Stand-Alone Wind/Photovoltaic/Fuel Cell Energy System Caisheng Wang, *Senior Member, IEEE*, and M. Hashem Nehrir, *Senior Member, IEEE*, IEEE TRANSACTIONS ON ENERGY CONVERSION, VOL. 23, NO. 3, SEPTEMBER 2008

[14] " Dynamic Maximum Power Point Tracking of Photovoltaic Arrays Using Ripple Correlation Control " Trishan Esram, W. Kimball, T. Krein, I EEE transaction on power electronics, VOL. 21, NO. 5, SEPTEMBER 2006

[15] Unit sizing and control of hybrid wind-solar power systems. IEEE Transactions on Energy Conversion, Vol. 12, No. 1, March 1997

[16] Designing of Hybrid Power Generation system using Wind energy-Photovoltaic Solar energy- Solar energy with Nan antenna (IJERA) Vol. 2, Issue 1, Jan-Feb 2012, pp.812-815

[17] Hybrid Wind-Fuel Cell Renewable Energy utilization Scheme for Village Electricity Mohamed A. H. El-Sayed, Adel M. Sharaf, Senior Member IEEE Proceedings of the 14thnternational Middle East Power Systems Conference (MEPCON'10), Cairo University, Egypt, December 19-21, 2010, Paper ID 132

[18] HYBRID WIND-SOLAR ENERGY Nitesh, suraj kumar, abhishek humar, Undergraduate Academic Research Journal (UARJ), ISSN: 2278 – 1129, Volume-1, Issue-3, 4, 2012

[19] Sustained power generation by Dynamic Modeling of wind/fuel cell/ultra-capacitor-based hybrid power generation system Nilesh K. Meshram , Shubhas Y. Kamdi IRJES *e- ISSN :2319-183X, p-ISSN :* 2319-1821

[20] Comparison between Batteries and Fuel Cells for Photovoltaic System Backup, M. Sedighizadeh, and A. Rezazadeh, PWASET VOLUME 26 DECEMBER 2007 ISSN 1307-6884.

[21] Optimal Sizing of a Hybrid Wind/PV Plant Considering Reliability Indices S. Dehghan, B. Kiani, A. Kazemi, A. Parizad, World Academy of Science, Engineering and Technology 32 2009